Cotransport of human adenoviruses with clay colloids and TiO$_2$ nanoparticles in saturated porous media: Effect of flow velocity

Vasiliki I. Syngouna [a,*], Constantinos V. Chrysikopoulos [a], Petros Kokkinos [b],
Maria A. Tselepi [b], Apostolos Vantarakis [b]

[a] School of Environmental Engineering, Technical University of Crete, 73100 Chania, Greece
[b] Environmental Microbiology Unit, Department of Public Health, University of Patras, 26500 Patras, Greece

HIGHLIGHTS

- The transport of adenovirus in saturated porous media was affected by clays and TiO$_2$ NPs.
- Adenovirus retention by packed columns was highest in the presence of TiO$_2$ NPs.
- No distinct relationship between adenovirus retention and flow rate was established.
- Collision efficiencies during cotransport were shown to increase with flow rate.

GRAPHICAL ABSTRACT
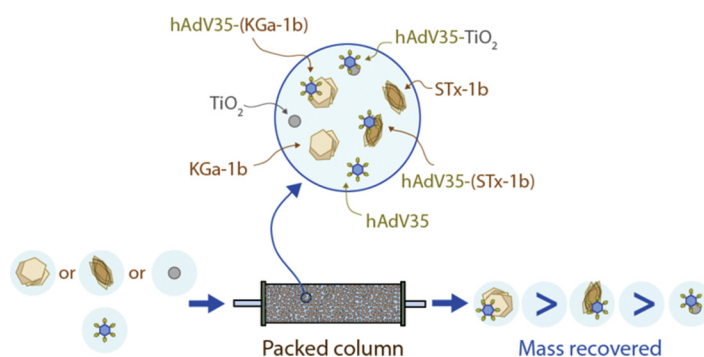
ARTICLE INFO

ABSTRACT

This study focuses on the effects of two clay colloids (kaolinite, KGa-1b and montmorillonite, STx-1b) and titanium dioxide (TiO$_2$) nanoparticles (NPs) on human adenovirus transport and retention in water saturated porous media at three different pore water velocities (0.38, 0.74, and 1.21 cm/min). Transport and cotransport experiments were performed in 30-cm long laboratory columns packed with clean glass beads with 2 mm diameter. The experimental results suggested that the presence of KGa-1b, STx-1b and TiO$_2$ NPs increased human adenovirus inactivation and attachment onto the solid matrix, due to the additional attachment sites available. Retention by the packed column was found to be highest (up to 99%) in the presence of TiO$_2$ NPs at the highest pore water velocity, and lowest in the presence of KGa-1b. The experimental results suggested that adenoviruses would undergo substantial aggregation or heteroaggregation during cotransport. However, no distinct relationships between mass recoveries and water velocity could be established from the experimental cotransport data. Note that for the cotransport experiments, collision efficiency values were shown to be higher for the higher flow rate examined in this study.

© 2017 Elsevier B.V. All rights reserved.

1. Introduction

Pathogenic viruses are present in aquifers, groundwater wells, and drinking water due to improper wastewater disposal operations (Zhuang and Jin, 2008; Weaver et al., 2013; Sadeghi et al., 2013;

* Corresponding author.
  E-mail address: vsyngouna@isc.tuc.gr (V.I. Syngouna).

Frohnert et al., 2014; Pang et al., 2014). Consequently, numerous experimental and theoretical studies published in the literature have investigated how virus fate and transport can be affected by various physicochemical factors (Jin et al., 2000; Walshe et al., 2010; Sadeghi et al., 2011). Also, our group has previously investigated how virus transport can be influenced by environmental parameters such as fluid velocity (Syngouna and Chrysikopoulos, 2011; Kokkinos et al., 2015), matrix structure (Masciopinto et al., 2008), moisture content (Sim and Chrysikopoulos, 2000; Anders and Chrysikopoulos, 2009), grain size (Anders and Chrysikopoulos, 2005; Syngouna and Chrysikopoulos, 2011), gravity (Chrysikopoulos and Syngouna, 2014), and presence of suspended clays (Syngouna and Chrysikopoulos, 2013, 2015, 2016; Katzourakis and Chrysikopoulos, 2014). It should be noted, however, that most of these studies use bacteriophages as surrogates for human viruses.

Clay particles are the most abundant inorganic colloids in aquatic systems (Cai et al., 2014; Wilson et al., 2014) and could serve as carriers of viruses, by facilitating or hindering their mobility in environmental systems (Walshe et al., 2010; Syngouna and Chrysikopoulos, 2015). Clay particles consist mainly of stacks of two-dimensional aluminosilicate layers: silicon dioxide tetrahedral sheets (T) and aluminum oxyhydroxyl octahedral sheets (O). Montmorillonite and kaolinite are typical examples of T—O—T and T—O clay particles, respectively (van Olphen, 1963).

Titanium dioxide (TiO_2) nanoparticles (NPs) are widely used nanomaterials (materials with at least one external dimension in the size range 1–100 nm) in consumer products (e.g. cosmetic and skin care products, pigments, wastewater treatment compounds, catalysts). Due to their widespread use in household and industrial commodities, TiO_2 NPs have been accidentally or intentionally released into natural soils and waters (Robichaud et al., 2009; Lin et al., 2010; Chowdhury et al., 2012; Cai et al., 2014; Keller and Lazareva, 2013). The production of TiO_2 in the United States alone is expected to increase to ~2.5 million tons/year by 2025 (Robichaud et al., 2009). Additionally, the concentration of Ti in municipal wastewater treatment plant effluents is in the range of 10–100 mg/L (Kiser et al., 2009). The TiO_2 NPs properties (e.g. high surface area, small size, surface chemistry, electrical properties) may be altered when dispersed in natural environments and their transport in porous media may be affected by environmental conditions (Fang et al., 2009; Chen et al., 2011; Chowdhury et al., 2011; Godinez and Darnault, 2011; Sygouni and Chrysikopoulos, 2015). Moreover, TiO_2 NPs have shown a strong tendency to attach onto biocolloids (e.g. bacteria, viruses) (Chowdhury et al., 2012; Schwegmann et al., 2013; Gentile and Fidalgo de Cortalezzi, 2016), and have demonstrated to have antimicrobial properties in the presence of light (photocatalysis) (Li et al., 2008; Schwegmann et al., 2013). However, it is worthy to note that the transport of human adenoviruses in the presence of clay colloids and TiO_2 NPs in the subsurface is not fully understood.

Viruses, and human adenoviruses in particular, are commonly found in the aquatic environment due to their disinfection resistance, and in aging drinking water and wastewater treatment systems that are vulnerable to pathogen intrusion. Many studies have investigated the influence of just a single environmental variable on human adenovirus inactivation and attachment onto porous media (e.g. flow velocity, temperature, clay presence) (Wong et al., 2012; Pang et al., 2014; Kokkinos et al., 2015; Bellou et al., 2015). To our knowledge, to date, there has been no study on human adenovirus transport in saturated porous media in the presence of clay colloids and TiO_2 NPs. Certainly, this work is a substantial extension of the work conducted by Kokkinos et al. (2015), who studied the effect of flow velocity on the transport of human adenoviruses. Column experiments were conducted using glass beads as the column packing material in order to eliminate possible experimental difficulties associated with real soil, which may provide numerous uncertainties that can considerably complicate the analysis of the experimental data. Human adenoviruses, which are more resistant to disinfection than enteroviruses or rotaviruses, were chosen as the most suitable virus surrogates.

2. Materials and methods

2.1. Clay colloids

The clays used in this study were kaolinite (KGa-1b, a well-crystallized kaolin from Washington County, Georgia) and montmorillonite (STx-1b, a Ca-rich montmorillonite, white, from Gonzales County, Texas), purchased from the Clay Minerals Society, Columbia, USA. Fifty grams of each clay mineral were mixed with 100 mL distilled deionized water (ddH_2O) in a 2-L beaker. Sufficient hydrogen peroxide (30%, solution) was added to oxidize all organic matter. The mineral suspension was adjusted to pH 10 with 0.1 M NaOH solutions and dispersed by ultrasonication for 20 min. The suspension was diluted to 2 L and the <2 μm colloidal fraction was separated by sedimentation. The separated colloid suspension was flocculated by adding 0.5 M $CaCl_2$ solution. The colloidal particles were washed with ddH_2O and ethanol to remove the Cl^- ions and subsequently dried at 60 °C (Rong et al., 2008). The <2 μm colloidal fraction was diluted in a low ionic strength (I_S) sterile DNase-I reaction buffer solution (pH = 7.6, I_S = 1.4 mM) to the desirable concentration (51.38 ± 2.26 mg/L and 51.11 ± 2.15 mg/L for KGa-1b and STx-1b, respectively) for all transport and cotransport experiments conducted in this study. Dynamic light scattering (DLS) (ZetaSizerNano-ZS90 analyzer, Malvern Instrument Inc., U.K.) was used to measure the <2 μm colloidal fraction of KGa-1b equal to 0.84 ± 0.13 μm, and STx-1b equal to 1.19 ± 0.38 μm. Furthermore, transmission electron microscopy (TEM) analyses by JEOL (JEM-2100 system, operated at 200 kV) suggested that the KGa-1b particle size was in the range of 0.2–1 μm and the average size of STx-1b particles equal to 0.5 μm (Chrysikopoulos and Syngouna, 2012). The optical density of the clay colloids was analyzed at a wavelength of 280 nm by a UV–vis spectrophotometer, and the corresponding clay concentrations were determined by the standard calibration curves of clay optical densities (see Fig. S1a, b of Supporting data), which are based on dry weights.

2.2. Titanium dioxide suspensions

TiO_2 NP powder (anatase, <25 nm in diameter, purity > 99.9%) was purchased from Sigma-Aldrich Corporation. The crystalline composition of the TiO_2 NP powder "as shipped" (or untreated), was determined to be a pure anatase phase, by using X-ray diffraction (XRD) analysis (Bruker D8 advance diffractometer with Ni-filtered CuKα radiation and a LynxEye detector). The corresponding XRD pattern was obtained at a 2θ range from 2° to 70°, scanned at a scanning angle increment of 0.015° with a time step of 0.3 s. The XRD analysis suggested that the TiO_2 anatase crystallite size is equal to 20.8 nm. A stock TiO_2 NPs suspension (1000 mg/L) was prepared by mixing TiO_2 nanopowder with Milli-Q distilled deionized water (ddH_2O). The mixture was sonicated for 30 min in order to obtain a relatively homogenized and monodispersed TiO_2 NPs suspension. The size distribution of TiO_2 NPs in ddH_2O, was determined after settling for a period of 7 days using dynamic light scattering (DLS) (ZetaSizer Nano-ZS90 analyzer, Malvern Instrument Inc., U.K.) and was found to be 180 ± 31 nm. This value was comparable to the previously reported hydrodynamic diameter of TiO_2 NP aggregates (Mukherjee and Weaver, 2010; Chen et al., 2011). Transmission electron microscopy (TEM) with JEOL (JEM-2100 system, operated at 200 kV), was performed by diluting a NPs suspension in ddH_2O, which was subsequently placed in an ultrasonic bath for 10 min, and air-dried onto a carbon-coated copper grid (200 mesh). The TEM analysis also indicated the presence of many stable aggregates of the primary nanoparticles (see Fig. S2 of the Supporting data). At the same time, the unsettled TiO_2 NPs suspension in ddH_2O was diluted in sterile DNase-I reaction buffer solution (pH = 7.6, I_S = 1.4 mM) to achieve a concentration of 25.69 ± 1.05 mg/L, which was used in the subsequent transport and cotransport experiments. The constant TiO_2 NP concentration was chosen because it has been reported in the literature that

at $I_S = 1.0$ mM, greater elution of TiO_2 NPs occurs with increasing particle concentrations (Chowdhury et al., 2011). The optical density of the TiO_2 NPs was analyzed at a wavelength of 287 nm with a UV–vis spectrophotometer, and the corresponding TiO_2 NP concentrations were determined with the standard calibration curve of TiO_2 optical densities, which is based on dry weights. Using the calibration curve (see Fig. S1c of the Supporting data), each measured TiO_2 absorbance, $A_{(TiO_2)}$ [−], was converted to TiO_2 concentration, $C_{(TiO_2)}$ [mg/L].

2.3. Cell cultures

The human adenovirus serotype 35 strain (hAdV35) was cultivated in human lung carcinoma cell line A549 growing in Dulbecco's modified Eagle's medium (DMEM; Gibco, Grand Island, NY, U.S.) containing 4.5 g/L D-Glucose, L-glutamine and pyruvate with 10% heat inactivated fetal bovine serum (FBS; Gibco). A549 cells support the replication of most human adenovirus serotypes, except of the fastidious serotypes 40 and 41. For the preparation of virus stocks, A549 cells were cultured in 175-cm² flasks at 37 °C, in an atmosphere of 5% CO_2 to 80–90% confluence, and infected with hAdV35. Subsequently, the hAdVs were released from cells by freezing and thawing the culturing flasks 3 times. A centrifugation step at 3000 ×g for 20 min was applied to eliminate cell debris. The supernatant was collected and ultracentrifuged for 1 h at 34,500 ×g, and finally re-suspended in PBS, quantified and stored in 10-mL aliquots at −80 °C. The initial concentration of hAdV35 stock was quantified by Real-Time PCR and recorded at 10^6 genome copies/mL.

All A549 cell monolayers were incubated overnight in 12–well plates (Cellstar, Greiner bio-one) at 37 °C, in an atmosphere of 5% CO_2 to 90–100% confluence. Thirty microliters (30 μL) of direct and diluted samples were inoculated for 90 min at 37 °C on an Orbital Shaker–Incubator (ES-20, Biosan). Media with inoculate were discarded, and DMEM media supplemented with 1% FBS were added. The flasks were incubated for 3–4 days at 37 °C in 5% CO_2 and then examined for cytopathic effects (CPE). Cytotoxicity effects were determined by visual inspection under the optical microscope. The final results were expressed as the geometric mean of the most probable number of cytopathic units (MPNCU) per milliliter, calculated for two independent replicates. All assays were performed in triplicate, and negative and positive controls were included.

2.4. Virus real time PCR assay

For hAdVs molecular detection, the conserved region of the hexon gene was used as the target area. The hAdVs were quantified by real-time PCR (qPCR). A neat and a 10-fold dilution of the virus nucleic acid extract were tested. All samples were tested in duplicates (two neat and two diluted). The primers and probes for quantification of hAdVs were adopted from Hernroth et al. (2002). The qPCR assays were performed using TaqMan Universal PCR Master Mix (Applied Biosystems) and a carry-over contamination prevention system, uracil N-glycosylase. In each assay, 10 μL sample of nucleic acid extract was added, to a final reaction volume of 25 μL. For each plate, the genome copies (GC/mL) were measured. Ultra-pure water was used as the non-template control for each assay. Real-Time PCR was carried out for 2 min at 50 °C with preheating for 10 min at 95 °C, followed by 45 - cycles of PCR amplification (denaturation at 95 °C for 15 s, annealing and extension at 60 °C for 1 min) (Hernroth et al., 2002). The assay was designed to quantify all common human adenoviruses, and was proven to be highly specific for hAdV35 detection and quantification (Bofill-Mas et al., 2013). The lower detection limit was previously reported to be 10 GC/mL (Bofill-Mas et al., 2006; Carducci and Verani, 2013). The equation of the calibration curve used in this study was: FAM (6-fluorescein amidite); $y = -3.38 \times \log_{10}(x) + 38.39$; efficiency E = 97.8%. All virus assays were performed in duplicate. Additional quality control analyses were performed by a cultivation method (Carratalà

et al., 2013). Note that, it was important to exclude the effect of virus inactivation when evaluating interactions of viruses with clay colloids and TiO_2 NPs under the present experimental conditions. Previous batch inactivation experiments under identical experimental conditions in the presence and absence of clays suggested that no significant virus inactivation is expected over the experimental duration. However, in the presence of clays, it was unclear whether the viruses were inactivated and attached onto clays, or if the virus populations were not homogeneous, where some viruses could be more resistant than others (Bellou et al., 2015).

2.5. Column experiments

Column experiments were performed using a 30-cm long glass column with 2.5 cm diameter. The column was packed with 2 mm diameter sterile purified glass beads under standing sterile DNase-I reaction buffer solution. Following the procedure described by Syngouna and Chrysikopoulos (2013), the glass beads were purified until the water conductivity was negligible. Briefly, the beads were cleaned with concentrated 0.1 M HNO_3 (70%) for 3 h to remove surface impurities, rinsed with ddH_2O, soaked in 0.1 M NaOH for 3 h, and then rinsed with ddH_2O again. After cleaning, the glass beads were dried in an oven at 105 °C, and then stored in screw cap sterile beakers. The dry bulk density was estimated to be $\rho_b = 1.61$ g/cm³, and the porosity $\theta = 0.42 \pm 0.01$. The column was placed horizontally to minimize gravity effects (Chrysikopoulos and Syngouna, 2014). A new column was packed for each experiment. Also, three pore volumes (PVs) of sterile Dnase-I reaction buffer solution were passed through the column prior to each transport experiment. The entire packed column and glassware used for the experiments were sterilized in an autoclave at 121 °C for 20 min. Constant flow of a buffer solution at three flow rates of Q = 2.5, 1.5, and 0.8 mL/min, corresponding to specific discharge or approach velocities of q = 0.51, 0.31, and 0.16 cm/min, and pore water (interstitial) velocities of U = q/θ = 1.21, 0.74, and 0.38 cm/min, respectively, was maintained with a peristaltic pump (Masterflex L/S, Cole-Palmer). Typically, the movement of groundwater is quite slow, on the order of less than one foot per day to a few tens of feet per day. It should be noted that the higher pore water velocities employed in this work represent site remediation processes under forced flow conditions, while the lowest pore water velocity is quite low and thus representative of slow sand filtration and field conditions. For both single particle transport and cotransport of particles (clay colloids, TiO_2 NPs) with human adenoviruses, the influent suspensions were injected into the packed column for 3 PVs, followed by 3 PVs of buffer solution. All experiments were carried out at room temperature (~25 °C). The effluent total suspended virus concentrations, $C_{Total-v}$ [M/L^3] (suspended virus, C_v, plus virus sorbed onto suspended particles, C_{vp}), were quantified by qPCR. Effluent suspended particle concentrations, C_p [M/L^3] were measured by UV absorbance at wavelengths of 280 nm and 287 nm for clay colloids and TiO_2 NPs, respectively.

2.6. Analysis of experimental data

The attachment of hAdV35 onto glass beads, clay colloids and TiO_2 NPs was evaluated using the classical colloid filtration theory (CFT). The dimensionless collision efficiency, α (the ratio of the collisions resulting in attachment to the total number of collisions between suspended particles and collector grains), was calculated for each breakthrough curve with the following expression (Rajagopalan and Tien, 1976):

$$\alpha = -\frac{2d_c \ \ln\left(M_{r(i)}/M_{r(t)}\right)}{3(1-\theta)\eta_0 L} \tag{1}$$

where d_c [L] is the average collector diameter, L [L] is the length of the packed column, θ [−] is the porosity, $M_{r(i)}$ [−] is the mass recovery in

the outflow of the suspended viruses or particles i; $M_{r(t)}$ [−] is the tracer mass recovery in the outflow, quantified by the following expression (James and Chrysikopoulos, 2011):

$$M_{r(i)}(L) = \frac{\int_0^\infty C_i(L, t)dt}{\int_0^{t_p} C_i(0, t)dt} \qquad (2)$$

where C_i is either the total suspended virus or particle concentration in the outflow. The required dimensionless single-collector removal efficiency in Eq. (1), η_0 [−], was predicted by an existing correlation equation (Tufenkji and Elimelech, 2004), which depends on the non-dimensional Peclet, number, N_{Pe}, Gravity number, N_G, van der Waals number, N_{vdW}, attraction number, N_A, and relative size number, N_R. For the cotransport experiments, the apparent collision efficiency introduced by Walshe et al. (2010), $\alpha_{Total-v}$ [−], based on the total virus concentration, $C_{Total-v}$ [M/L³], in the outflow, was calculated using Eqs. (1), (2) and considering the particle modified glass beads at the first stages of particle influx as the initial "clean collector" (Syngouna and Chrysikopoulos, 2013; Gentile and Fidalgo de Cortalezzi, 2016). The required parameters for calculating the collision efficiency, single-collector removal efficiency, and deposition rate coefficient for hAdV35, clay colloids, and TiO₂ NPs were calculated from the transport and cotransport experimental data. These parameters are presented in Table S1 of Supplementary data.

3. Results and discussion

3.1. Particle transport experiments

Fig. 1 shows the normalized breakthrough data at each flow rate (2.5, 1.5, 0.8 mL/min) for the three particles (KGa-1b, STx-1b, and TiO₂ NPs) considered in this study. Note that previous electrokinetic measurements, under identical experimental conditions, revealed that the different particles employed in this study were negatively charged (Syngouna and Chrysikopoulos, 2013, 2017). Therefore, the retention of these particles by the also negatively charged glass beads was not expected to be significant (see Electrokinetic Measurements section in Supporting data). However, some retention was observed, especially for clay colloids. Non-DLVO Lewis acid-base interactions and hydrogen bonds could also be partially responsible for the observed retention. The calculated M_r values, are listed in Table 1. With no exception, all estimated M_r values for both clay colloids (KGa-1b, STx-1b) were significantly lower than those of TiO₂ NPs. Note that the Brownian motion of TiO₂ NPs is higher than that of clay colloids due to their smaller size, which potentially increases the probability of collisions between TiO₂ NPs and glass beads (Dunphy Guzman et al., 2006; Fang et al., 2009). The observed higher retention of KGa-1b compared to STx-1b could be attributed to its higher hydrophobicity (Syngouna and Chrysikopoulos, 2013). There are several factors responsible for the observed higher retention of clay colloids than TiO₂ NPs in the packed column. First, there exist higher attraction forces between glass beads and clay colloids than glass beads and TiO₂ NPs. Second, larger sized clay colloids or aggregates do not pass through the pores (size exclusion) as freely as the TiO₂ NPs. Third, clay colloids attach more than TiO₂ NPs onto previously deposited particles, due to the presence of stronger attraction forces among them. TiO₂ NP aggregates are expected to behave somewhat differently than colloid particles (Fang et al., 2009). Furthermore, TiO₂ NP aggregates may be subject to shear forces that could break up aggregates (Dunphy Guzman et al., 2006). Note that all three types of particles used in this study were suspended in low ionic strength Dnase-I reaction buffer, thus repulsion was dominant (see Figs. S3 and S4 in Supporting data). Straining could occur even if the ratio of particle to glass bead diameter is <0.002, and may be another possible physical removal mechanism independent of electrostatic interactions (Bradford et al., 2002). Moreover, higher retention of both clay colloids and TiO₂ NPs by the packed column was observed at the lowest flow rate (see Fig. 1,
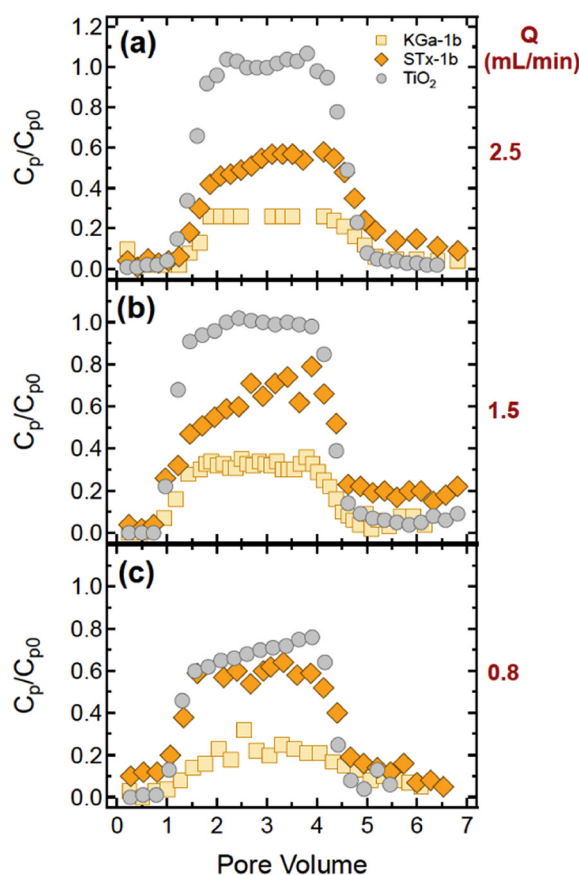
Fig. 1. Experimental effluent normalized concentrations from the transport of KGa-1b (squares), STx-1b (diamonds) and TiO₂ NPs (circles) experiments. Here Q equal to: (a) 2.5, (b) 1.5, and (c) 0.8 mL/min.

Table 1), suggesting that hydrodynamics possibly had greater influence on the detachment than the attachment process. Worthy to note is that, lower flow rate would result in more efficient Brownian diffusion transport to collector surface (Lecoanet and Wiesner, 2004), and greater colloid deposition (Bradford et al., 2007). Under similar experimental conditions, Godinez and Darnault (2011) observed that an increase in flow velocity enhanced the transport of TiO₂ NPs. However, no distinct relationship between mass recoveries and flow rate could be established from the particle transport experimental results of this study.

3.2. Virus particle cotransport experiments

Fig. 2 shows the normalized breakthrough data for the cotransport of hAdV35 with KGa-1b, STx-1b and TiO₂ NPs, at three flow rates (2.5, 1.5, 0.8 mL/min), together with the breakthrough data for the transport of hAdV35, which were collected by Kokkinos et al. (2015). Note that the total virus concentrations represent the sum of suspended viruses and viruses sorbed onto suspended particles ($C_{Total-v} = C_v + C_{vp}$). The M_r values based on $C_{Total-v}$ and C_p in the effluent for hAdV35, KGa-1b, STx-1b and TiO₂ NPs, for all three flow rates (Q = 2.5, 1.5, 0.8 mL/min), are listed in Table 1. The transport characteristics of hAdV35 were highly affected by the presence of both clay colloids and TiO₂ NPs. Higher hAdV35 retention by the packed column was observed in the presence of clay colloids and TiO₂ NPs, than in the absence of clays and TiO₂ NPs (see Fig. 2). This is probably a consequence of the formation of large clay-virus and TiO₂-virus aggregates that clogged the pores (Chowdhury et al., 2012), as well as clay-bound and TiO₂-bound viruses retained by the column due to clay and TiO₂ attachment onto glass beads (Syngouna and Chrysikopoulos, 2013, 2015). Furthermore, hAdV35 deposition onto glass beads, clays, and TiO₂ NPs could be

Table 1
Measured and calculated parameter values for particle transport and virus-particle co-transport experiments.

Q (mL/min)	C_{v0} GC/mL	C_{p0} mg/L	M_r $C_{Total-v}$ (%)	M_r C_p (%)	$\alpha_{Total-v}$	α_p
Particle transport experiments						
Adenovirus (hAdV35) (Kokkinos et al., 2015)						
2.5	2130734		25.9		0.77	
1.5	483231		32.8		0.43	
0.8	1094559		24		0.35	
Kaolinite (KGa-1b)						
2.5		52.1		29.4		1
1.5		53.8		36.5		0.68
0.8		51.2		28		0.43
Montmorillonite (STx-1b)						
2.5		53.8		73.3		0.2
1.5		51.9		87		0.13
0.8		48.4		71.3		0.16
TiO₂ NPs						
2.5		27.3		100		0.01
1.5		25.5		100		0.01
0.8		24.6		75		0.08
Virus-particle cotransport experiments						
Adenovirus (hAdV35)-kaolinite (KGa-1b)						
2.5	55034	47.3	10	13.4	1	1
1.5	69824	52.8	15.18	37.7	0.73	0.64
0.8	139715	51.1	6.08	33.7	0.68	0.36
Adenovirus (hAdV35)-montmorillonite (STx-1b)						
2.5	105361	49.6	8.43	25.8	1	0.85
1.5	127894	50	3.6	22.2	1	0.59
0.8	87986	53.1	4.01	19.5	0.81	0.31
Adenovirus (hAdV35)-TiO₂ NPs						
2.5	231094	25	0.638	28	1	1
1.5	192986	26.7	5.89	39	1	0.74
0.8	220351	25.1	1.8	45.7	1	0.36

enhanced due to the high isoelectric point of hAdV35 (Shi et al., 2012; Wong et al., 2014). However, hAdV35 viruses may attach onto clays or TiO₂ NPs tightly during an initial pseudo-equilibrium period, but subsequently gradually detach (Davidson et al., 2013; Syngouna and Chrysikopoulos, 2010). Similar to the particle transport experiments, straining seems to be an important removal mechanism. Syngouna and Chrysikopoulos (2013), under similar experimental conditions,

observed lower retention of bacteriophages MS2 and ΦX174 than hAdV35 in the presence of clay colloids (KGa-1b, STx-1b). Also, the inactivation rate of bacteriophages was reported to be slower than that of hAdV35 (Bellou et al., 2015; Magri et al., 2015). Moreover, the inactivation mechanism may be different for MS2 viruses (with simple structure containing RNA) than that of hAdV35 (with complex structure containing DNA). It should be noted that no distinct relationship between hAdV35 mass recovery and flow rate could be established from the virus-particle cotransport experimental results.

Fig. 3 illustrates the various M_r values for the hAdV35 cotransport experiments with three different flow rates (2.5, 1.5, 0.8 mL/min). The M_r values for hAdV35 were higher in the presence of KGa-1b (6.08–15.18%) than STx-1b (3.60–8.43%) or TiO₂ NPs (0.64–5.89%). Note that, at flow rate 2.5 mL/min, about 99% of the hAdV35 particles were removed by the packed column in the presence of TiO₂ NPs. Bellou et al. (2015) suggested that hAdV35 attachment onto bentonite and kaolinite was affected by the type of clay mineral. Note that, attached hAdV35 viruses may be both viable and inactivated. Furthermore, the inactivation rates of suspended and attached viruses may be different (Gerba, 1984; Sim and Chrysikopoulos, 1996). However, Bellou et al. (2015) reported that, under practically identical experimental conditions to those employed in this study, no significant hAdV35 inactivation could be observed neither in the presence nor the absence of clays. In the presence of TiO₂ NPs the possibility of hAdV35 inactivation by breaching of the capsid, followed by radical attack to DNA and core proteins, should not be eliminated (Liga et al., 2013). The lowest virus retention was observed in the presence of KGa-1b. The highest virus mass recovery was M_r = 15.18% in the presence of KGa-1b at the flow rate of Q = 1.5 mL/min. Overall, the location of clay particles and TiO₂ NPs within the pores of the packed column, as well as their morphologies may have contributed to the observed increase of hAdV35 retention. Pang et al. (2014) reported reversible as well as irreversible attachment of human adenovirus, but only reversible attachment of MS2 during transport in sand media. Although it is not unrealistic to hypothesize that hAdV35 viruses can be detached from clays and TiO₂ NPs, additional research is required to fully describe the associated mechanisms.

Fig. 4 shows the normalized cotransport breakthrough data for the three selected particles (KGa-1b, STx-1b and TiO₂ NPs) in the presence and absence of hAdV35. The presence of hAdV35 affected the transport
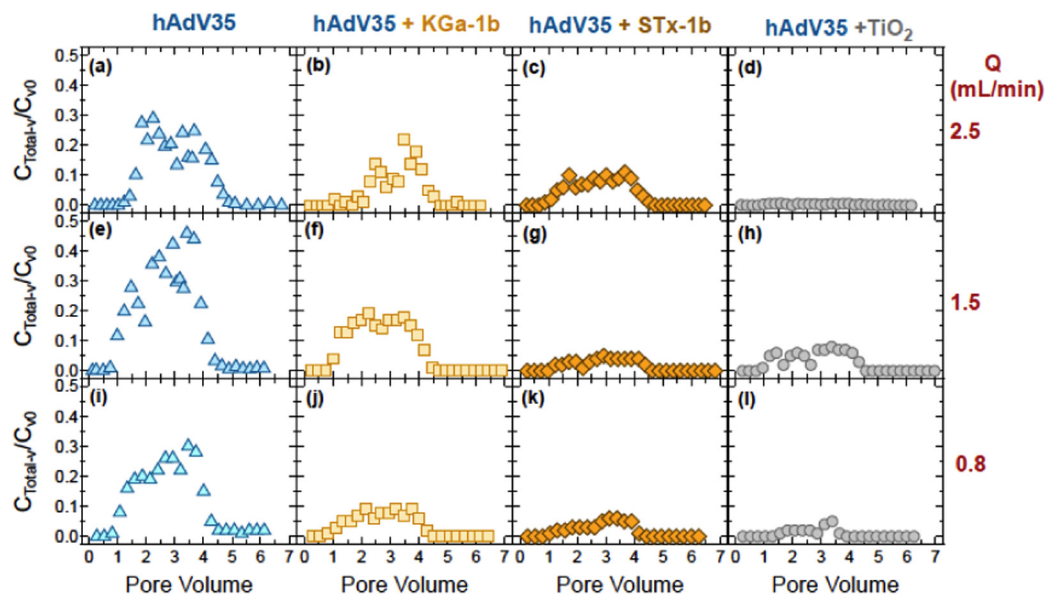
Fig. 2. Breakthrough data from the hAdV35 transport experiments (a, e, i) (Kokkinos et al., 2015), and the hAdV35 cotransport experiments with: (b, f, j) KGa-1b, (c, g, k) STx-1b, and (d, h, l) TiO₂ NPs. Here Q equals to: (a–d) 2.5, (e–h) 1.5, and (i–l) 0.8 mL/min.
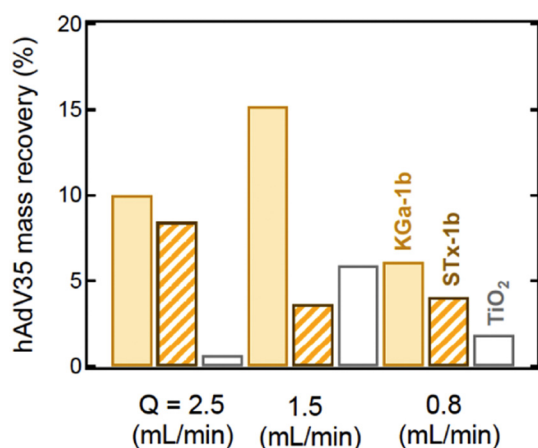
Fig. 3. Calculated M_r values for the hAdV35 cotransport experiments with: KGa-1b (solid bars), STx-1b (cross-shaded bars), and TiO$_2$ NPs (open bars), for three different flow rates (Q = 2.5, 1.5, and 0.8 mL/min).

of all particles, but mostly the TiO$_2$ NPs (see Table 1). The retention of all particles by the packed column was highly increased in the presence of hAdV35, probably due to formation of particle-hAdV35 aggregates. The clay colloids and TiO$_2$ NPs attached onto the glass beads may be responsible for adhering incoming viruses (Gentile and Fidalgo de Cortalezzi, 2016). The M_r of all particles (KGa-1b, STx-1b and TiO$_2$ NPs) was substantially reduced in the presence of hAdV35, but not affected by the flow rate (see Table 1). However, in contrast, Cai et al. (2016) observed that the copresence of bacteria increased the transport and decreased the deposition of TiO$_2$ NPs in columns packed with quartz sand. The cotransport experimental data show that $C_{Total-v}$ of hAdV35 (see Fig. 2) and C_p of KGa-1b, STx-1b and TiO$_2$ NPs (see Fig. 4) are considerably reduced in the outlet, possibly due to heteroaggregation.

The collision efficiency values, $\alpha_{Total-v}$ and α_p based on $C_{Total-v}$ and C_p, respectively, were calculated with Eq. (1) for all three flow rates, and they are listed in Table 1 for both transport and cotransport experiments. The $\alpha_{Total-v}$ holds information about the adsorption of $C_{Total-v}$ onto glass beads (transport experiments) and the adsorption of $C_{Total-v}$

onto glass beads and particles previously attached onto the glass beads (cotransport experiments). Note that all estimated collision efficiency values above unity were set equal to 1. Collision efficiency values above unity are theoretically impossible, but those between 1 and 1.25 are not considered rare. Discrepancies between the actual shape of collectors and the perfect spheres can cause these overestimated values (Gentile and Fidalgo de Cortalezzi, 2016). Note that, high values of collision efficiency factors suggest coexistence of straining along with physicochemical filtration (Jaisi et al., 2008). The $\alpha_{Total-v}$ values for the hAdV35 transport experiments (see Fig. 5a) were lower than the α_p values for the KGa-1b transport experiments (see Fig. 5b), but higher than α_p values for the STx-1b and TiO$_2$ NPs transport experiments (see Fig. 5c and d, respectively), for all flow rates. The α_p values were lowest for TiO$_2$ NPs transport experiments, for all flow rates. The $\alpha_{Total-v}$ values for the hAdV35 cotransport experiments were higher than those in transport experiments, for all cases examined (see Fig. 5a). Higher $\alpha_{Total-v}$ values were observed for hAdV35 in the presence of TiO$_2$ NPs than clay colloids (KGa-1b, STx-1b), for all flow rates (see Table 1), which could be attributed to the greater affinity of hAdV35 for TiO$_2$ nanoparticles. Note that, viruses attached onto TiO$_2$ were inactivated faster than those suspended in the aqueous phase. Virus inactivation may be enhanced in the proximity of newly generated hydroxyl radicals (OH•) (Liga et al., 2011), and has been found to be directly proportional to virus attachment onto TiO$_2$ (Koizumi and Taya, 2002). The solution chemistry as well as the presence of ionizable residues on virus surfaces can affect the interaction between viruses and TiO$_2$ (Liga et al., 2013; Syngouna and Chrysikopoulos, 2017). Similar α_p values for KGa-1b were observed for both the transport and cotransport experiments (see Fig. 5b), while the estimated α_p values for STx-1b and TiO$_2$ NPs were shown to be higher for the cotransport than the transport experiments (see Fig. 5c, d). Note that for the cotransport experiments, both $\alpha_{Total-v}$ and α_p values were shown to be higher for the higher flow rate examined in this study.

4. Conclusions

The outcomes from this study provided some insights on the influence of clay colloids (KGa-1b, STx-1b) and TiO$_2$ nanoparticles on the transport and retention of human adenoviruses (hAdV35) in water
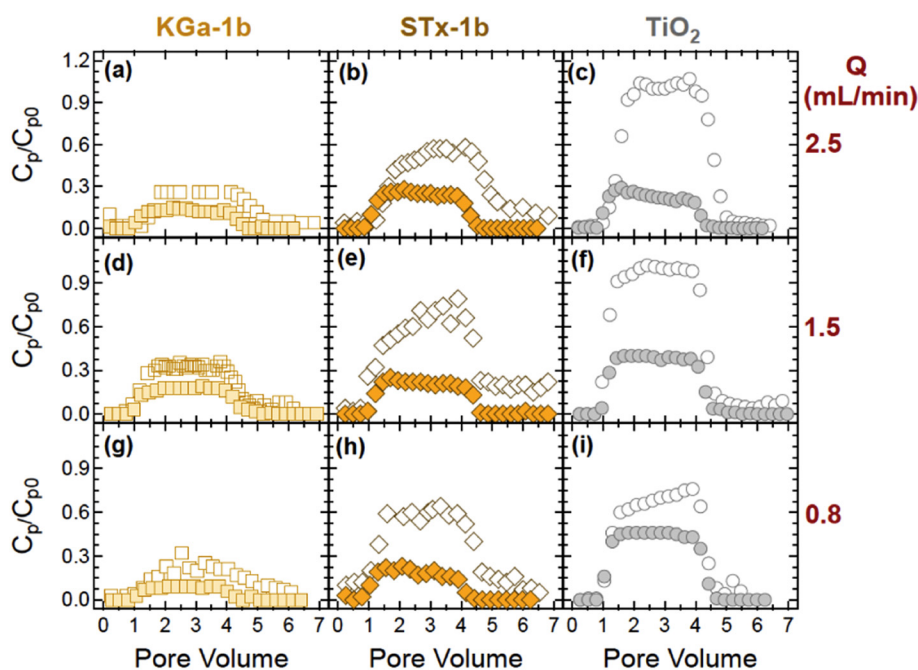
Fig. 4. Comparison of effluent normalized concentrations from the transport (open symbols) and cotransport (filled symbols) experiments with: (a, d, g) KGa-1b (squares), (b, e, h) STx-1b (diamonds) and (c, f, i) TiO$_2$ NPs (circles). Here Q equals to: (a–c) 2.5, (d–f) 1.5, and (g–i) 0.8 mL/min.
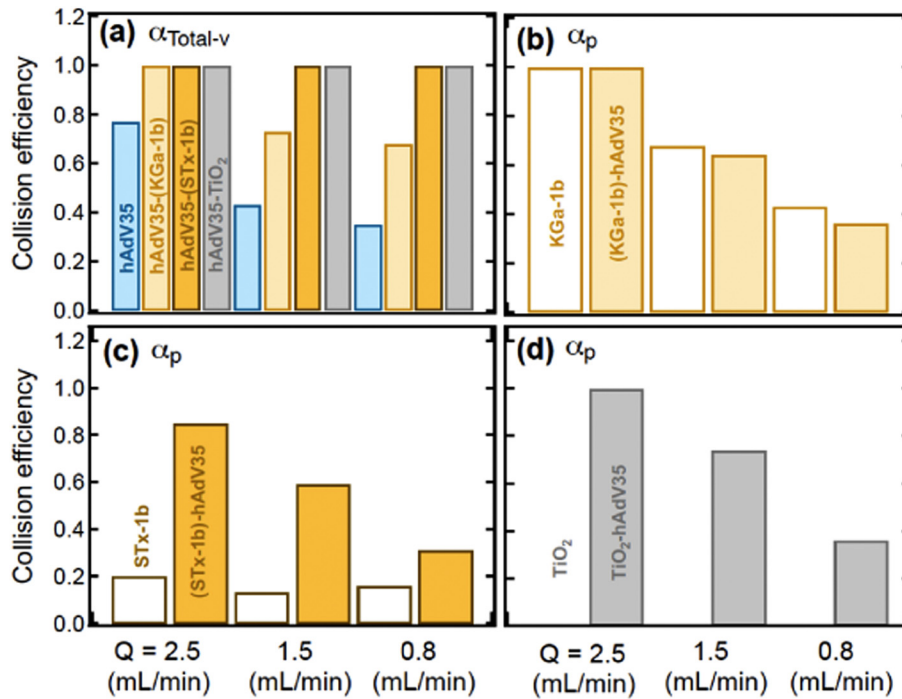
Fig. 5. Comparison of: (a) $\alpha_{Total-v}$ for HAdV35, (b) α_p for KGa-1b, (c) α_p for STx-1b, and (d) α_p for TiO$_2$ NPs for transport (open bars) and cotransport (solid bars) experimental data at three different Q values (Q = 2.5, 1.5, and 0.8 mL/min).

saturated laboratory scale columns, packed with glass beads. Mass recovery values for hAdV35, calculated based on total virus concentration in the effluent, were reduced compared to those in the absence of clays and nanoparticles. Higher hAdV35 retention in the packed column was observed in the presence of TiO$_2$ NPs than in the presence of KGa-1b and STx-1b. The retention of hAdV35 particles was significant, up to 99%, in the presence of TiO$_2$ NPs at the flow rate of Q = 2.5 mL/min. A combination of straining due to heteroaggregation of hAdV35 and clay colloids or TiO$_2$ NPs, and previously deposited particles were responsible for the observed increased retention. The experimental results have shown that the transport of hAdV35 in saturated porous media was severely hampered, mostly by the presence of TiO$_2$ NPs. Consequently, these nanomaterials can be used as enhancer in drinking water sand filters, or as a mean for retention of pathogenic viruses during remediation processes.

Appendix A. Supplementary data

Supplementary data to this article can be found online at http://dx.doi.org/10.1016/j.scitotenv.2017.04.082.

References

Anders, R., Chrysikopoulos, C.V., 2005. Virus fate and transport during artificial recharge with recycled water. Water Resour. Res. 41, W10415. http://dx.doi.org/10.1029/2004WR003419.

Anders, R., Chrysikopoulos, C.V., 2009. Transport of viruses through saturated and unsaturated columns packed with sand. Transp. Porous Media 76, 121–138.

Bellou, M., Syngouna, V.I., Tselepi, M.A., Kokkinos, P.A., Paparrodopoulos, S.C., Chrysikopoulos, C.V., Vantarakis, A., 2015. Interaction of human adenovirus and coliphages with kaolinite and bentonite. Sci. Total Environ. 517, 86–95.

Bofill-Mas, S., Albinana-Gimenez, N., Clemente-Casares, P., Hundesa, A., Rodriguez-Manzano, J., Allard, A., Calvo, M., Girones, R., 2006. Quantification and stability of human adenoviruses and polyomavirus JC PyV in wastewater matrices. Appl. Environ. Microbiol. 72 (12), 7894–7896.

Bofill-Mas, S., Rusiñol, M., Fernandez-Cassi, X., Carratalà, A., Hundesa, A., Girones, R., 2013. Quantification of human and animal viruses to differentiate the origin of the fecal contamination present in environmental samples. Biomed. Res. Int. http://dx.doi.org/10.1155/2013/19208.

Bradford, S.A., Yates, S.R., Bettahar, M., Simunek, J., 2002. Physical factor affecting the fate and transport of colloid in saturated porous media. Water Resour. Res. 38, 1327–1338.

Bradford, S.A., Torkzaban, S., Walker, S.L., 2007. Coupling of physical and chemical mechanisms of colloid straining in saturated porous media. Water Res. 41, 3012–3024.

Cai, L., Tong, M., Wang, X., Kim, H., 2014. Influence of clay particles on the transport and retention of titanium dioxide nanoparticles in quartz sand. Environ. Sci. Technol. 48 (13), 7323–7332.

Cai, L., Peng, S., Wu, D., Tong, M., 2016. Effect of different-sized colloids on the transport and deposition of titanium dioxide nanoparticles in quartz sand. Environ. Pollut. 208, 637–644.

Carducci, A., Verani, M., 2013. Effects of bacterial, chemical, physical and meteorological variables on virus removal by a wastewater treatment plant. Food Environ. Virol. 5 (1), 69–76.

Carratalà, A., Rodriguez-Manzano, J., Hundesa, A., Rusiñol, M., Fresno, S., Cook, N., Girones, R., 2013. Effect of temperature and sunlight on the stability of human adenoviruses and MS2 as fecal contaminants on fresh produce surfaces. Int. J. Food Microbiol. 164, 128–134.

Chen, G., Liu, X., Su, C., 2011. Transport and retention of TiO$_2$ rutile nanoparticles in saturated porous media under low-ionic-strength conditions: measurements and mechanisms. Langmuir 27, 5393–5402.

Chowdhury, I., Hong, Y., Honda, R.J., Walker, S.L., 2011. Mechanisms of TiO$_2$ nanoparticle transport in porous media: role of solution chemistry, nanoparticle concentration, and flowrate. J. Colloid Interf. Sci. 360 (2), 548–555.

Chowdhury, I., Cwiertny, D.M., WalkerS, L., 2012. Combined factors influencing the aggregation and deposition of nano-TiO$_2$ in the presence of humic acid and bacteria. Environ. Sci. Technol. 46, 6968–6976.

Chrysikopoulos, C.V., Syngouna, V.I., 2012. Attachment of bacteriophages MS2 and FX174 onto kaolinite and montmorillonite: extended-DLVO interactions. Colloids Surf. B Biointerfaces 92, 74–83.

Chrysikopoulos, C.V., Syngouna, V.I., 2014. Effect of gravity on colloid transport through water-saturated columns packed with glass beads: modeling and experiments. Environ. Sci. Technol. 48, 6805–6813.

Davidson, P.C., Kuhlenschmidt, T.B., Bhattarai, R., Kalita, P.K., Kuhlenschmidt, M.S., 2013. Investigation of rotavirus survival in different soil fractions and temperature conditions. J. Environ. Prot. 4, 1–9.

Dunphy Guzman, K.A., Finnegan, M.P., Banfield, J.F., 2006. Influence of surface potential on aggregation and transport of titania nanoparticles. Environ. Sci. Technol. 40, 7688–7693.

Fang, J., Shan, X.Q., Wen, B., Lin, J.M., Owens, G., 2009. Stability of titania nanoparticles in soil suspensions and transport in saturated homogeneous soil columns. Environ. Pollut. 157, 1101–1109.

Frohnert, A., Apelt, S., Klitzke, S., Chorus, I., Szewzyk, R., Selinka, H.C., 2014. Transport and removal of viruses in saturated sand columns under oxic and anoxic conditions—potential implications for groundwater protection. Int. J. Hygiene Environ. Health 217 (8), 861–870.

Gentile, G.J., Fidalgo de Cortalezzi, M.M., 2016. Enhanced retention of bacteria by TiO$_2$ nanoparticles in saturated porous media. J. Contam. Hydrol. 191, 66–75.

Gerba, C.P., 1984. Applied and theoretical aspects of virus adsorption to surfaces. Adv. Appl. Microbiol. 30, 133–168.

Godinez, I.G., Darnault, C.J.G., 2011. Aggregation and transport of nano-TiO$_2$ in saturated porous media: effects of pH, surfactants and flow velocity. Water Res. 45 (2), 839–851.

Hernroth, B.E., Conden-Hansson, A.C., Rehnstam-Holm, A.S., Girones, R., Allard, A.K., 2002. Environmental factors influencing human viral pathogens and their potential indicator organisms in the blue mussel, Mytilus edulis: the first Scandinavian report. Appl. Environ. Microbiol. 68 (9), 4523–4533.

Jaisi, D.P., Saleh, N.B., Blake, R.E., Elimelech, M., 2008. Transport of single-walled carbon nanotubes in porous media: filtration mechanisms and reversibility. Environ. Sci. Technol. 42 (22), 8317–8323.

James, S.C., Chrysikopoulos, C.V., 2011. Monodisperse and polydisperse colloid transport in water-saturated fractures with various orientations: gravity effects. Adv. Water Resour. 34 (10), 1249–1255.

Jin, Y., Pratt, E., Yates, M., 2000. Effect of mineral colloids on virus transport through saturated sand columns. J. Environ. Qual. 29, 532–540.

Katzourakis, V.E., Chrysikopoulos, C.V., 2014. Mathematical modeling of colloid and virus cotransport in porous media: application to experimental data. Adv. Water Resour. 68, 62–73.

Keller, A.A., Lazareva, A., 2013. Predicted releases of engineered nanomaterials: from global to regional to local. Environ. Sci. Technol. Lett. 1 (1), 65–70.

Kiser, M.A., Westerhoff, P., Benn, T., Wang, Y., Perez-Rivera, J., Hristovski, K., 2009. Titanium nanomaterial removal and release from wastewater treatment plants. Environ. Sci. Technol. 43 (17), 6757–6763.

Koizumi, Y., Taya, M., 2002. Kinetic evaluation of biocidal activity of titanium dioxide against phage MS2 considering interaction between the phage and photocatalyst particles. Biochem. Eng. J. 12, 107–116.

Kokkinos, P., Syngouna, V.I., Tselepi, M.A., Bellou, M., Chrysikopoulos, C.V., Vantarakis, A., 2015. Transport of human adenoviruses in water saturated laboratory columns. Food Environ. Virol. 7 (2), 122–131.

Lecoanet, H.F., Wiesner, M.R., 2004. Velocity effects on fullerene and oxide nanoparticle deposition on porous media. Environ. Sci. Technol. 38, 4377–4382.

Li, Q., Mahendra, S., Lyon, D.Y., Brunet, L., Liga, M.V., Li, D., Alvarez, P.J.J., 2008. Antimicrobial nanomaterials for water disinfection and microbial control: potential applications and implications. Water Res. 42 (18), 4591–4602.

Liga, M.V., Bryant, E.L., Colvin, V.L., Li, Q., 2011. Virus inactivation by silver doped titanium dioxide nanoparticles for drinking water treatment. Water Res. 45, 535–544.

Liga, M.V., Maguire-Boyle, S.J., Jafry, H.R., Barron, A.R., Li, Q., 2013. Silica decorated TiO$_2$ for virus inactivation in drinking water — simple synthesis method and mechanisms of enhanced inactivation kinetics. Environ. Sci. Technol. 47 (12), 6463–6470.

Lin, D., Tian, X., Wu, F., Xing, B., 2010. Fate and transport of engineered nanomaterials in the environment. J. Environ. Qual. 39, 1896–1908.

Magri, M.E., Fidjeland, J., Jönsson, H., Albihn, A., Vinnerås, B., 2015. Inactivation of adenovirus, reovirus and bacteriophages in fecal sludge by pH and ammonia. Sci. Total Environ. 520, 213–221.

Masciopinto, C., La Mantia, R., Chrysikopoulos, C.V., 2008. Fate and transport of pathogens in a fractured aquifer in the Salento area, Italy. Water Resour. Res. 44 (1), W01404. http://dx.doi.org/10.1029/2006WR005643.

Mukherjee, B., Weaver, J.W., 2010. Aggregation and charge behavior of metallic and nonmetallic nanoparticles in the presence of competing similarly-charged inorganic ions. Environ. Sci. Technol. 44 (9), 3332–3338.

van Olphen, H., 1963. An Introduction to Clay Colloid Chemistry. Interscience, New York.

Pang, L., Farkas, K., Bennett, G., Varsani, A., Easingwood, R., Tilley, R., Nowostawska, U., Lin, S., 2014. Mimicking filtration and transport of rotavirus and adenovirus inn sand media using DNA-labeled, protein-coated silica nanoparticles. Water Res. 62, 167–179.

Rajagopalan, R., Tien, C., 1976. Trajectory analysis of deep-bed filtration with the sphere-in-cell porous media model. AICHE J. 22 (3), 523–533.

Robichaud, C.O., Uyar, A.E., Darby, M.R., Zucker, L.G., Wiesner, M.R., 2009. Estimates of upper bounds and trends in nano-TiO$_2$ production as a basis for exposure assessment. Environ. Sci. Technol. 43, 4227–4233.

Rong, X., Huanga, Q., He, X., Chen, H., Cai, P., Liang, W., 2008. Interaction of Pseudomonas putida with kaolinite and montmorillonite: a combination study by equilibrium adsorption, ITC, SEM and FTIR. Colloids Surf. B Biointerfaces 64 (1), 49–55.

Sadeghi, G., Schijven, J.F., Behrends, T., Hassanizadeh, S.M., Gerritse, J., Kleingeld, P.J., 2011. Systematic study of effects of pH and ionic strength on attachment of phage PRD1. Ground Water 49 (1), 12–19.

Sadeghi, G., Schijven, J.F., Behrends, T., Hassanizadeh, S.M., van Genuchten, M.T., 2013. Bacteriophage PRD1 batch experiments to study attachment, detachment and inactivation processes. J. Contam. Hydrol. 152, 12–17.

Schwegmann, H., Ruppert, J., Frimmel, F.H., 2013. Influence of the pH-value on the photocatalytic disinfection of bacteriawith TiO$_2$ — explanation by DLVO and XDLVO theory. Water Res. 47 (4), 1503–1511.

Shi, C.J., Wei, J., Jin, Y., Kniel, K.E., Chiu, P.C., 2012. Removal of viruses and bacteriophages from drinking water using zero-valent iron. Sep. Purif. Technol. 84, 72–78.

Sim, Y., Chrysikopoulos, C.V., 1996. One-dimensional virus transport in porous media with time dependent inactivation rate coefficients. Water Resour. Res. 32 (8), 2607–2611.

Sim, Y., Chrysikopoulos, C.V., 2000. Virus transport in unsaturated porous media. Water Resour. Res. 36 (1), 173–179.

Syngouna, V.I., Chrysikopoulos, C.V., 2010. Interaction between viruses and clays in static and dynamic batch systems. Environ. Sci. Technol. 44 (12):4539–4544. http://dx.doi.org/10.1021/es100107a.

Sygouni, V., Chrysikopoulos, C.V., 2015. Characterization of TiO$_2$ nanoparticle suspensions in aqueous solutions and TiO$_2$ nanoparticle retention in water-saturated columns packed with glass beads. Chem. Eng. J. 262, 823–830.

Syngouna, V.I., Chrysikopoulos, C.V., 2011. Transport of biocolloids in water saturated columns packed with sand: effect of grain size and pore water velocity. J. Contam. Hydrol. 126, 301–314.

Syngouna, V.I., Chrysikopoulos, C.V., 2013. Cotransport of clay colloids and viruses in water saturated porous media. Colloids Surf. A 416, 56–65.

Syngouna, V.I., Chrysikopoulos, C.V., 2015. Experimental investigation of virus and clay particles cotransport in partially saturated columns packed with glass beads. J. Colloid Interf. Sci. 440, 140–150.

Syngouna, V.I., Chrysikopoulos, C.V., 2016. Cotransport of clay colloids and viruses through water-saturated vertically oriented columns packed with glass beads: gravity effects. Sci. Total Environ. 545–546, 210–218.

Syngouna, V.I., Chrysikopoulos, C.V., 2017. Inactivation of MS2 bacteriophage by titanium dioxide nanoparticles in the presence of quartz sand with and without ambient light. J. Colloid Interf. Sci. 497, 117–125.

Tufenkji, N., Elimelech, M., 2004. Correlation equation for predicting single-collector efficiency in physicochemical filtration in saturated porous media. Environ. Sci. Technol. 38 (2), 529–536.

Walshe, G.E., Pang, L., Flury, M., Close, M.E., Flintoft, M., 2010. Effects of pH, ionic strength, dissolved organic matter, and flow rate on the cotransport of MS2 bacteriophages with kaolinite in gravel aquifer media. Water Res. 44, 1255–1269.

Weaver, L., Sinton, L.W., Pang, L., Dann, R., Close, M., 2013. Transport of microbial tracers in clean and organically contaminated silica sand in laboratory columns compared with their transport in the field. Sci. Total Environ. 443, 55–64.

Wilson, M.J., Wilson, L., Patey, I., 2014. The influence of individual clay minerals on formation damage of reservoir sandstones: a critical review with some new insights. Clay Miner. 49, 147–164.

Wong, K., Mukherjee, B., Kahler, A.M., Zepp, R., Molina, M., 2012. Influence of inorganic ions on aggregation and adsorption behaviors of human adenovirus. Environ. Sci. Technol. 46 (20), 11145–11153.

Wong, K., Bouchard, D., Molina, M., 2014. Relative transport of human adenovirus and MS2 in porous media. Colloids Surf. B: Biointerfaces 122, 778–784.

Zhuang, J., Jin, Y., 2008. Interactions between viruses and goethite during saturated flow: effects of solution pH, carbonate, and phosphate. J. Contam. Hydrol. 98 (1–2), 15–21.